

Temperature-responded tunable metalenses based on phase transition materials

Jing-Jun Wu(伍景军), Feng Tang(唐烽), Jun Ma(马骏), Bing Han(韩冰), Cong Wei(魏聪), Qing-Zhi Li(李青芝), Jun Chen(陈骏), Ning Zhang(张宁), Xin Ye(叶鑫), Wan-Guo Zheng(郑万国), and Ri-Hong Zhu(朱日宏)

Citation: Chin. Phys. B, 2022, 31 (**5**): 054216. DOI: 10.1088/1674-1056/ac3cad
Journal homepage: http://cpb.iphy.ac.cn; http://iopscience.iop.org/cpb

What follows is a list of articles you may be interested in

Laser-induced damage threshold in HfO_2/SiO_2 multilayer films irradiated by *β*-ray

Mei-Hua Fang(方美华), Peng-Yu Tian(田鹏宇), Mao-Dong Zhu(朱茂东), Hong-Ji Qi(齐红基), Tao Fei(费涛), Jin-Peng Lv(吕金鹏), Hui-Ping Liu(刘会平)

Chin. Phys. B, 2019, 28 (**2**): 024215. DOI: 10.1088/1674-1056/28/2/024215

Influence of low-temperature sulfidation on the structure of ZnS thin films

Shuzhen Chen(陈书真), Ligang Song(宋力刚), Peng Zhang(张鹏), Xingzhong Cao(曹兴忠), Runsheng Yu(于润升), Baoyi Wang(王宝义), Long Wei(魏龙), Rengang Zhang(张仁刚)

Chin. Phys. B, 2019, 28 (**2**): 024214. DOI: 10.1088/1674-1056/28/2/024214

Experimental demonstration of narrow-band rugate minus filters using rapidly alternating deposition technology

Ying Zhang(章瑛), Yan-Zhi Wang(王胭脂), Jiao-Ling Zhao(赵娇玲), Jian-Da Shao(邵建达), Shuang-Chen Ruan(阮双琛)

Chin. Phys. B, 2018, 27 (**5**): 054217. DOI: 10.1088/1674-1056/27/5/054217

Effects of annealing time on the structure, morphology and stress of gold-chromium bilayer film

Hong Zhang(张洪), Yun-Xia Jin(晋云霞), Hu Wang(王虎), Fang-Yu Kong(孔钒宇), Hao-Peng Huang(黄昊鹏), Yun Cui(崔云)

Chin. Phys. B, 2016, 25 (**10**): 104205. DOI: 10.1088/1674-1056/25/10/104205

An improved transmitting multi-layer thin-film filter

Zhang Ying, Qi Hong-Ji, Yi Kui, Wang Yan-Zhi, Sui Zhan, Shao Jian-Da

Chin. Phys. B, 2015, 24 (**5**): 054212. DOI: 10.1088/1674-1056/24/5/054212

Temperature-responded tunable metalenses based on phase transition materials

Jing-Jun Wu(伍景军)[1,2,3], Feng Tang(唐烽)[3], Jun Ma(马骏)[1,2], Bing Han(韩冰)[1,2], Cong Wei(魏聪)[1,2], Qing-Zhi Li(李青芝)[3], Jun Chen(陈骏)[3], Ning Zhang(张宁)[3], Xin Ye(叶鑫)[3,†], Wan-Guo Zheng(郑万国)[4,‡], and Ri-Hong Zhu(朱日宏)[1,2,§]

[1] *School of Electronic and Optical Engineering, Nanjing University of Science and Technology, Nanjing* 210094, *China*
[2] *MIIT Key Laboratory of Advanced Solid Laser, Nanjing University of Science and Technology, Nanjing* 210094, *China*
[3] *Research Center of Laser Fusion, China Academy of Engineering Physics, Mianyang* 621900, *China*
[4] *IFSA Collaborative Innovation Center, Shanghai Jiao Tong University, Shanghai* 200240, *China*

(Received 26 August 2021; revised manuscript received 15 November 2021; accepted manuscript online 24 November 2021)

Once the metalenses are fabricated, the functions of most metalenses are invariable. The tunability and reconfigurability are useful and cost-saving for metalenses in realistic applications. We demonstrate this tunability here via a novel hybrid metalens with the strategic placement of an ultra-thin VO_2 layer. The hybrid metalens is capable of dynamically modulating the focusing intensity of transmitted light at a wavelength of 1550 nm, and demonstrate a 42.28% focusing efficiency of the incident light and 70.01% modulation efficiency. The hybrid metalens' optothermal simulations show an optothermal conversion process of dynamic focusing, and a maximum laser density of 1.76×10^3 W/cm^2 can be handled at an ambient temperature lower than 330 K. The hybrid metalens proposed in this work, a light-dose sensitive tunable smart metalens that can protect other instruments/systems or materials from being damaged, has its specific applications such as in anti-satellite blinding, bio-imaging, *etc*.

Keywords: temperature-responded, tunable metalenses, phase change material VO_2

PACS: 42.79.Wc, 42.88.+h, 42.70.–a, 78.20.Bh **DOI:** 10.1088/1674-1056/ac3cad

1. Introduction

Lenses are one of the most important components in optical systems, such as cameras, microscopes, projective lithographic machines, spectrometers, triggering off a wide investigation of optics and photonics.[1] Traditional lenses based on refractive or reflective principles have some limitations in integration, weight, chromatic aberration, *etc*., which restricts the development of multifunctional optical devices.[2] Recently, metalens technology based on metasurfaces, which control the wavefront of light by using subwavelength nanostructures, has shown peculiar optical performance with micrometer thickness. Therefore, metalenses have been investigated widely to replace the bulk devices with thin, flat, lightweight devices.[3] However, the functions of most of metalenses are invariable once they are fabricated. For being harnessed in more applications with lower cost, the tunability of their performance becomes important.

To date, two common approaches have been exploited to tune metalenses. One is based on the reconfigurability of unit cells,[4,5] such as physical dimensions, interspace between unit-cells[6–8] and shapes,[9–11] to actively manipulate the output wavefront.[12] This tuning is typically accompanied by some forms of overall spatial variation of the devices, which, however, is not always desirable for some highly compact photonic devices.[3] The other is to integrate active materials into metalenses.[13] The active materials' optical properties can be tuned by external excitation, such as thermal,[14] electrical,[15] or optical stimuli.[12] Owing to the resonances of unit cells being highly sensitive to the dielectric background, the placed active material can control the metalenses' optical response. This allows the controlling of metalens without reconfiguring their structures.

Among these active materials, phase change and phase transition materials (PCMs and PTMs) are good candidates to provide widely tunable capabilities.[16] The PCM materials, such as germanium–antimony–tellurium (GST) and antimony sulfide (Sb_2S_3), are irreversible, that is, nonvolatile, and will remain in a fixed state of the matter unless an input excitation "resets" it back to its original state. Yin *et al.* proposed a bifocal zoom metalens, focusing position can be controlled actively according to the requirement.[17] Bai *et al.* designed an actively tunable metalens array by patterning the GST resonators. The metalenses array shows excellent broadband performance, and the "on" or "off" state of each metalens can be actively controlled manually.[18] Besides, Bai *et al.* designed a tunable duplex metalenses, which can focus the incident light

†Corresponding author. E-mail: yexin@caep.cn
‡Corresponding author. E-mail: group_ye@163.com
§Corresponding author. E-mail: zhurihong@njust.edu.cn

© 2022 Chinese Physical Society and IOP Publishing Ltd

at any position by actively controlling the state of GST.[19] Chen *et al.* designed multifunctional metalens with dual working modes based on bilayer geometric phase elements consisting of low-loss phase change materials (Sb_2Se_3) and amorphous silicon (a-Si).[20] The above-mentioned metalenses' focus position or intensities can be actively tuned to a great extent, but they are difficult to dynamically control in real-time due to PCMs requiring new excitation to "reset" it back to its original state.[16] The PTM material, *e.g.*, vanadium dioxide (VO_2), is naturally reversible and will return to its initial state if the external stimulus is discontinued. Therefore, VO_2 is more suitable for the equipment whose performance needs controlling in real-time, *e.g.*, intelligent temperature control systems. Recently, Chen *et al.* realized a reflected metalens in the far-infrared band by combining a geometrical metasurface and a VO_2 film.[21] The metasurfaces work as a reflective lens with a protective function from strong light. However, the tunable focusing and photothermal interaction of metalens have not been investigated previously.

In this paper, we propose a tunable metalens based on a hybrid structure combined with a VO_2 film and Si nanocylinders. The hybrid metalens works at 1550 nm and provide real-time tunability by using thin PTM layers. The temperature-dependent transmitted amplitude can be controlled within a certain range in which the system can work normally. Finally, the optothermal simulations are conducted to estimate the optothermal conversion progress of dynamic focusing, and the maximum laser density that the hybrid metalens can handle. The light-dose sensitive tunable smart metalens presents a new approach to the application of anti-satellite blinding, bioimaging, *etc*.

2. Materials and methods

Figure 1(a) shows the schematic diagram of our design. It comprises two films and an array of nanocylinder unit cells within a square lattice array. The materials of these layers from the bottom to the top are silicon oxide (SiO_2), vanadium oxide (VO_2), and silicon (Si), respectively. The period of unit cells is $P = 600$ nm. The nanocylinder's height is optimized to be $H = 750$ nm. The diameter of the nanocylinder is D. The phase difference of the transmitted light can be tuned by changing the diameter of nanocylinder. The optical components' phase profiles can be achieved by the unit cells of nanocylinders if the phase difference can cover the entire range of 0–2π. Nanocylinder is polarization independent due to its structural symmetry.[22]

In this study, the three-dimensional (3D) finite-difference time-domain method is used for optical simulations, and the discontinuous Galerkin time-domain method is used for thermal simulations. In optical simulations, the incident optical source is set to be a plane wave. The direction of propagation is along the z axis, and the polarization direction is along the x axis. The boundaries around the unit cell are periodic boundary conditions, and the top and bottom perfectly matches with the layer boundary conditions. The mesh accuracy is set to be 3. In thermal simulations, the x/y axis boundaries are set to be "closed", and the z axis boundaries are set to be "shell". The source and all objects are modeled as shown in Fig. 1(a) and limited in the optical/optothermal simulation region. The condition mode of boundaries is set to be the steady-state with a temperature of 330 K, and the temperature boundary is set to be at the bottom of the simulation region. The VO_2 permittivity's real and imaginary part are illustrated in Figs. A1(a) and A1(b) in Appendix A, respectively, and the data are cited from Ref. [23]. The constants of heat transport properties and electronic properties are cited from Refs. [24,25]. For the VO_2 material in an insulating state, the electrical conductivity, density, heat capacity, and thermal conductivity are set to be 221.8045 S/m, 4570 kg/m^3, 6560 J·kg^{-1}·K^{-1}, and 3.5 W·m^{-1}·K^{-1}, respectively. For the VO_2 material in a metallic state, the electrical conductivity, density, heat capacity, and thermal conductivity are set to be 94586.4662 S/m, 4650 kg/m^3, 7800 J·kg^{-1}·K^{-1}, and 6 W·m^{-1}·K^{-1}, respectively. The ambient temperature is set to be 330 K. The real parts and imaginary parts of SiO_2 and Si are cited from Ref. [26].

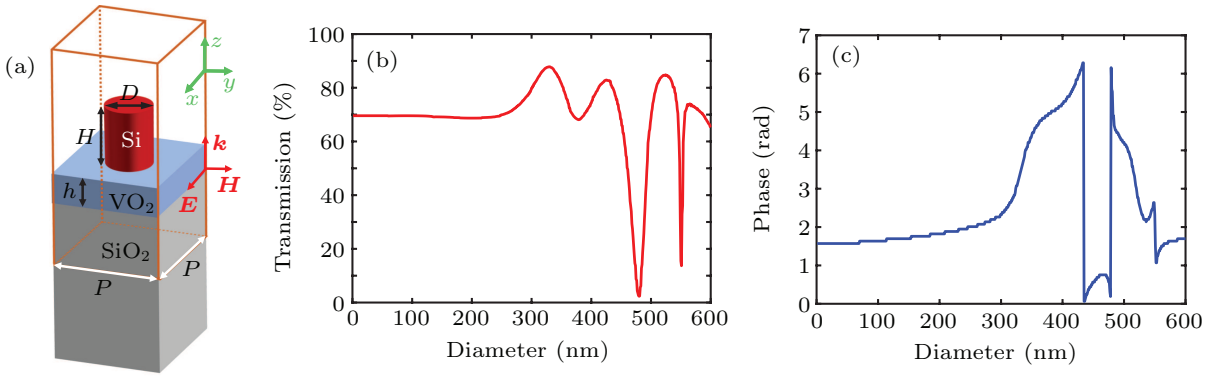


Fig. 1. Design of unit cells, showing (a) 3D view of unit cells, (b) transmission, and (c) phase for nanocylinders varying with nanocylinders' diameters.

3. Results and discussion

3.1. Optical properties of nanocylinders

The diameter-dependent transmission and phase difference of nanocylinders are illustrated in Figs. 1(b) and 1(c). The results ($\lambda = 1550$ nm) of unit cells can cover the entire range of 0–2π, which is the fundament of constructing metalens. In this research, the high transmission is obtained, when the height $H = 750$ nm, the lattice constant $P = 600$ nm. To realize the phase control of the metasurface (x, y) position, the appropriate diameters of the nanocylinders with high transmission in the range of 0–2π are selected. The phase modulation and the transmission corresponding to different nanocylinder sizes are shown in Table 1. These 8 high-transmission unit cells that entirely cover the range of 0–2π can be used to construct the metasurface.

Table 1. Dimensions of nanocylinders covering phase range of 0–2π.

Phase	0	$\pi/4$	$\pi/2$	$3\pi/4$	π	$5\pi/4$	$6\pi/4$	$7\pi/4$
T (%)	63.05	71.94	75.45	87.35	87.10	78.54	77.46	82.52
D (nm)	454.00	558.59	287.21	324.95	336.76	355.00	406.61	430.29

3.2. Metalens design and property

According to the phase profiles of metalens $\varphi(r\lambda) = -2\pi/\lambda(\sqrt{(r^2+f^2)}-f) + \varphi 0(\lambda)$, where λ is the target wavelength in vacuum, r is the radial distance to the metalens center, and f is the focal length, we construct a metalens operating at 1550 nm by using the above 8 selected nanocylinders. The metalens is constructed in the x–y plane, and the center is located at the coordinate origin. Therefore, $r^2 = x^2 + y^2$. Figure 2(a) represents the phase distribution of the metalens (with aperture $D = 87$ μm and focal length $f = 69.6$ μm). The constructed metalens is illustrated in Fig. 2(b) with the upper panels showing a top view, and the lower a side view). The partially enlarged details of the metalens, marked by the red box in Fig. 2(b), are shown in Fig. 2(c). The power distribution of the focusing spot on the x–z plane is illustrated in Fig. 2(d). The focal spot appears at the position of $z = 68.6756$ μm, which is slightly different from the designed 69.6 μm. This difference may be related to the position of the main plane of the metalens or the height of the nanocylinders.[27] The power distribution of the focusing spot on the x–y plane is shown in Fig. 2(e), and the power distribution with $y = 0$ μm, $z = 68.6756$ μm is illustrated in Fig. 2(f). The full-width at half maximum (FWHM) of the focal spot is 1.3951 μm. Figure 2(f) shows the focusing efficiency (the power in the focused spot 3× FWHM) of 42.28% for the incident light.

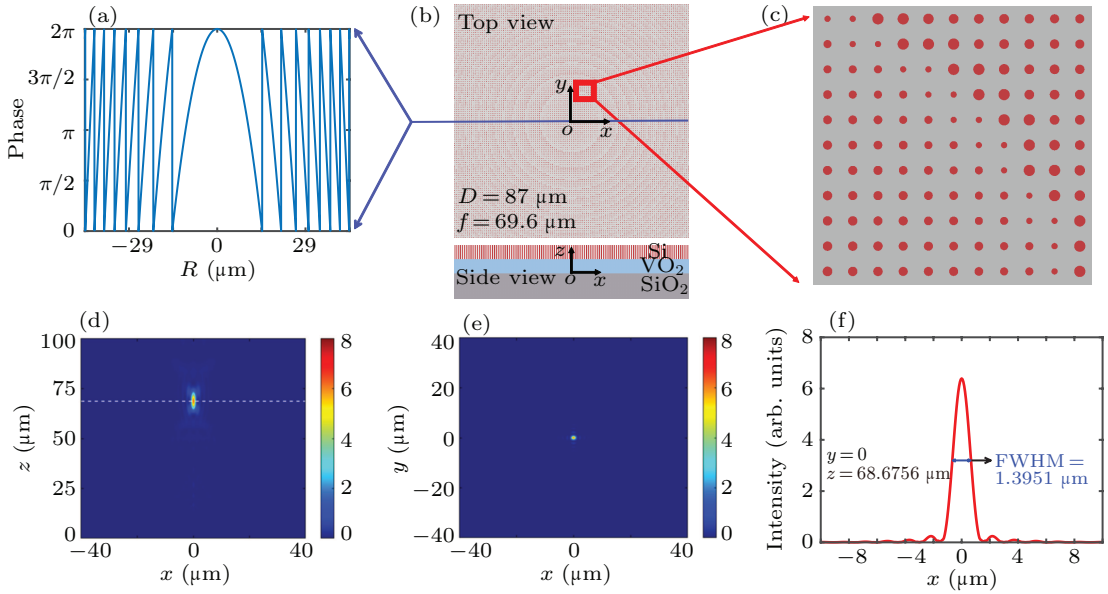


Fig. 2. Metalens construction and performance simulations, indicating (a) function of metalens phase distribution in a radial direction, (b) top and side view of metalens, (c) partially enlarged details of the metalens, marked by the red box in panel (b), (d) power distributions of the focusing spot in the x–z ($y = 0$ μm), (e) x–y ($z = 68.6756$ μm) plane, and (f) full width at half maximum (FWHM) of the focusing spot.

The dynamic focusing performance of the hybrid metalens is explored in detail as shown in Fig. 3. Figures 3(a)–3(f) show the power distributions of the focusing spot on the x–z plane at different temperatures (330 K, 339 K, 341 K, 343 K, 345 K, 350 K respectively). The power of the hybrid metalens focused spot gradually decreases as the temperature increases. It is seen that the focus wavelength of the hybrid metalens at different temperatures are almost the

same, focal distance $f = 68.6756$ μm. Figure 3(g) illustrates the power distributions of the focal point on the optical axis (white dashed line in Figs. 3(a)–3(f)). The FWHMs of the focal spots are almost the same when the temperature changes. It proves that the hybrid metalens proposed here can realize the dynamic focusing of the incident light. Because of our limited computer source, the diameter of metalens is set to be 87 μm. By increasing the diameter of the metalens, the FWHM can be miniaturized.[28] The transmission (T), reflection (R), absorption (A), and focusing efficiency (E) of the hybrid metalens at different temperatures are shown in Fig. 3(h). The T, R, and E of the hybrid metalens gradually decrease, and the A increases as the temperature increases. The T, R, and E are suppressed due to the strong absorption. As the temperature increases, the imaginary part of the VO_2 permittivity gradually increases, leading the absorption to increase sharply. The VO_2 appears in a full metallic state while the temperature is well above the transition temperature. Inhere, the T, R, and E of the hybrid metalens reach the highest values ($T = 59.09\%$, $R = 13.44\%$, $E = 42.28\%$) and the absorption reaches the lowest values ($A = 27.47\%$) at 330 K. While the hybrid metalens at 350 K, the T, R, and E reach the lowest values ($T = 17.25\%$, $R = 0.86\%$, $E = 12.68\%$) and the absorption reaches the highest values ($A = 81.89\%$). The modulation efficiency of T ($T_{350\ \mathrm{K}}/T_{330\ \mathrm{K}} - 1|$) is $\sim 70.81\%$, R ($|R_{350\ \mathrm{K}}/R_{330\ \mathrm{K}} - 1|$) is $\sim 93.60\%$, E ($|E_{350\mathrm{K}}/E_{330\ \mathrm{K}} - 1|$) is $\sim 70.01\%$, and A ($|A_{350\ \mathrm{K}}/A_{330\ \mathrm{K}} - 1|$) is 66.46%. As it can be seen that the hybrid metalens not only dynamically control the optical intensity, but also protect the speciesin measurement from being overe-exposed when the incident light is too strong.

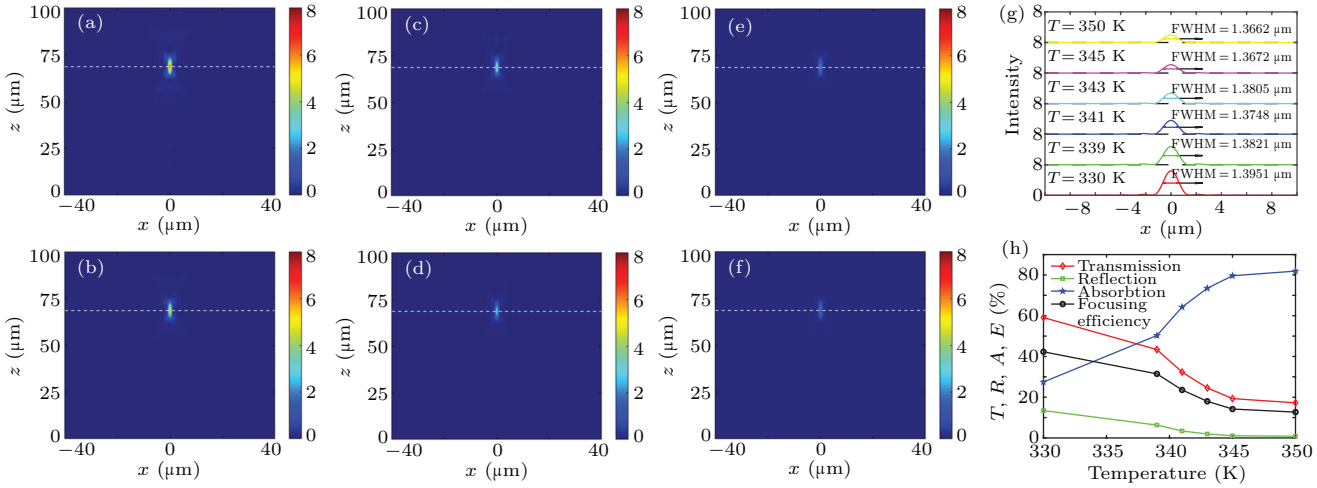


Fig. 3. Metalens properties at different temperatures: 330 K (a), 339 K (b), 341 K (c), 343 K (d), 345 K (e), 350 K (f), respectively, showing [(a)–(f)] power distributions of focusing spot in x–z ($y = 0$ μm) plane, with white dashed lines representing focal position, (g) FWHMs of focusing spots, (h) transmission (T), reflection (R), absorption (A), and focusing efficiency (E) of hybrid metalens.

Although the optical simulations can calculate the dynamic focusing efficiency of incident light with the increase of temperature, they cannot reflect the optothermal conversion process of dynamic focusing. For the quantitative analysis, some optothermal simulations are conducted to estimate the optothermal conversion process of the dynamic focusing, and the maximum light intensity that the hybrid metalens can handle. Figure 4(a) shows the temperature distribution in the hybrid metalens, composed of 19 selected unit cells in Table 1, illustrated by a plane-wave laser with power 3.64×10^{-10} W (the area is 0.6 μm $\times$11.4 μm = 6.84 μm). We simplify the original two-dimensional (2D) metalens ($D = 11.4$ μm, $f = 9.12$ μm) into a one-dimensional (1D) one, due to our limited computing source. The 1D hybrid metalens has a similar temperature value of 330 K while the laser power is lower than 3.64×10^{-10} W. Under the illumination of different incident power, the maximum temperature values in the three-dimensional (3D) volume made of the metalens are reported in Fig. 4(c). It is shown that the temperature of hybrid metalens increases gradually as the laser power is higher than 3.64×10^{-10} W, the laser density is 5.32×10^{-3} W/cm^2. Therefore, we believe that the hybrid metalens works normally while the ambient temperature is lower than 330 K and the incident light power is lower than 5.32×10^{-3} W/cm^2. As the laser energy increases, the temperature of the metalens gradually increases, and the VO_2 transits from the insulating state to the metallic state. It is usually considered that VO_2 is a fully metallic state while the temperature reaches 350 K, or even higher than 350 K. We suppose that the optical and thermal constants of VO_2, SiO_2, Si remain unchanged while the temperature is higher than 350 K. Figure 4(b) shows the temperature distribution in the hybrid metalens illustrated by a plane-wave laser with power 1.78×10^{-6} W. The temperature difference between the silicon nanocylinders and the VO_2 film is less than 1 K, just as the temperature is 330 K. The temperature of the hybrid metalens increases as the laser power increases as illustrated in Fig. 4(d). It is shown that the hybrid metalens can handle the maximum laser power (1.21×10^{-4} W per

6.84×10^{-8} cm^2), *i.e.*, the laser density is 1.76×10^3 W/cm^2. The melting point of Si, SiO_2, VO_2 are 1683 K, 1683 K, 1996 K, 1818 K respectively.

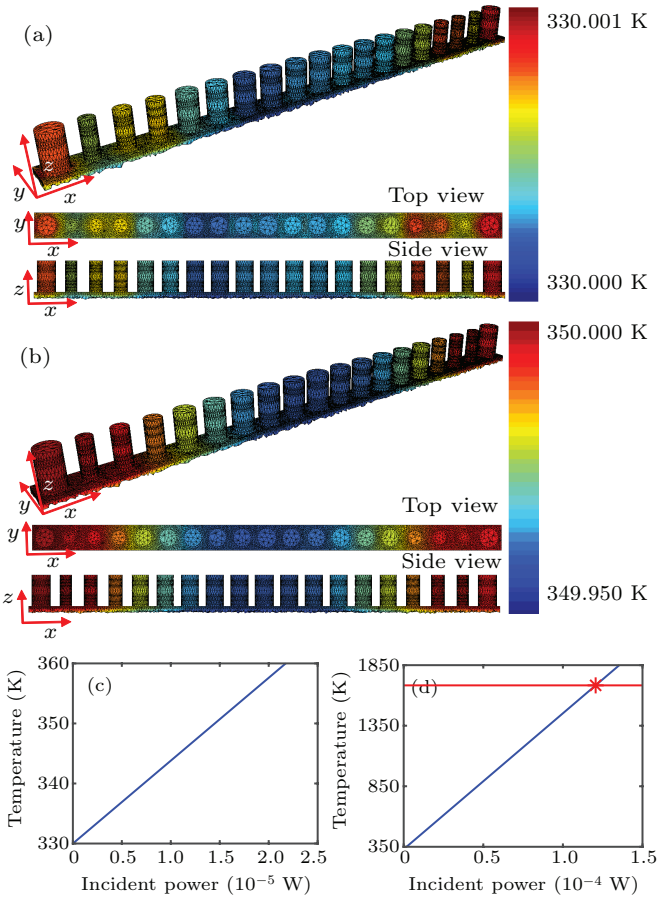


Fig. 4. Photothermal analysis of the hybrid metalens, indicating [(a), (b)] temperature distribution in 1D metalens (area: 6.84×10^{-8} cm^2) illustrated by plane-wave lasers with power 3.64×10^{-10} W and 1.78×10^{-6} W respectively, [(c), (d)] the highest temperature in 3D volume of panels (a) and (c) under the illumination of different incident powers respectively.

4. Conclusions and perspectives

In this work, we introduce a temperature-dependent tunable hybrid metalens operating at 1550 nm. Firstly, the geometrical dependence of the phase and transmittance of an Si nanocylinder is investigated. And then, a hybrid metalens is constructed and the temperature-dependent characteristics are simulated in detail. As the temperature increases, the focused power, transmission, reflection, and focusing efficiency of the hybrid metalens gradually decrease, and the absorption increases. The focusing efficiency of incident light and modulation efficiency of the focused efficiency are 42.28% and 70.01% respectively. Finally, the optothermal simulations illustrate the optothermal conversion progress of the dynamic focusing, and the hybrid metalens can handle a maximum laser density of 1.76×10^3 W/cm^2 at an ambient temperature lower than 330 K. We believe that the light-dose sensitive tunable smart metalens proposed in this work can provide a new practicable platform for realizing the instruments/systems or material damage protection, and potential applications in numerous technologically important fields such as anti-satellite blinding, bio-imaging, *etc*.

Acknowledgements

Project supported by the National Natural Science Foundation of China (Grant No. 61875087) and the Innovation and Development Foundation of China Academy of Engineering Physics (Grant No. CX20200020).

Appendix A: The figure cited from Ref. [23]

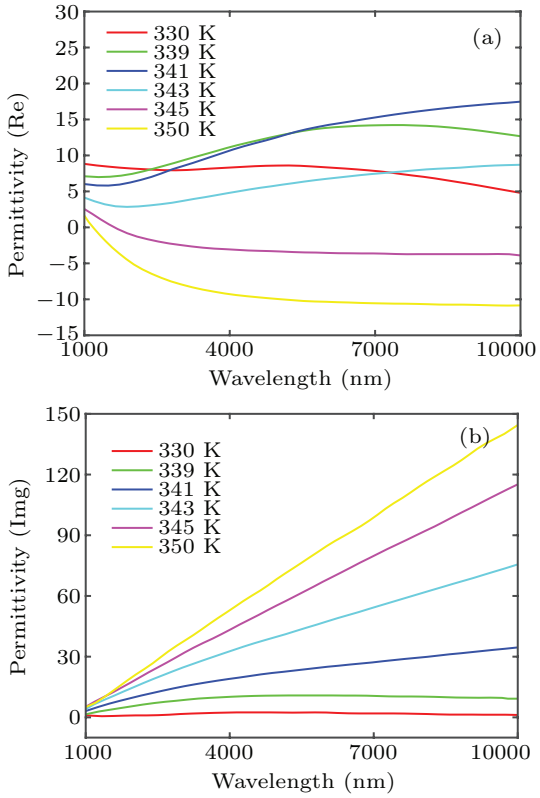


Fig. A1. Curves of (a) real part and (b) imaginary part *versus* wavelength of VO_2 permitivity data are cited from Ref. [23].

References

[1] Liu W, Cheng H, Tian J and Chen S 2020 *Adv. Phys. X* **5** 1742584
[2] Chen S, Li Z, Liu W, Cheng H and Tian J 2019 *Adv. Mater.* **31** 1802458
[3] He Q, Sun S and Zhou L 2019 *Research* **2** 1849272
[4] Ou J Y, Plum E, Zhang J and Zheludev N I 2013 *Nat. Nanotechnol.* **8** 252
[5] Zheludev N I and Plum E 2016 *Nat. Nanotechnol.* **11** 16
[6] Tao H, Strikwerda A C, Fan K, Padilla W J, Zhang X and Averitt R D 2009 *Phys. Rev. Lett.* **103** 147401
[7] Khodasevych I E, Shah C M, Sriram S, Bhaskaran M, Withayachumnankul W, Ung B S Y, Lin H, Rowe W S T, Abbott D and Mitchell A 2012 *Appl. Phys. Lett.* **100** 061101
[8] Ou J Y, Plum E, Jiang L and Zheludev N I 2011 *Nano Lett.* **11** 2142
[9] Zhu W M, Liu A Q, Zhang X M, Tsai D P, Bourouina T, Teng J H, Zhang X H, Guo H C, Tanoto H, Mei T, Lo G Q and Kwong D L 2011 *Adv. Mater.* **23** 1792
[10] Fu Y H, Liu A Q, Zhu W M, Zhang X M, Tsai D P, Zhang J B, Mei T, Tao J F, Guo H C, Zhang X H, Teng J H, Zheludev N I, Lo G Q and Kwong D L 2011 *Adv. Funct. Mater.* **21** 3589

[11] Powell D A, Hannam K, Shadrivov I V and Kivshar Y S 2011 *Phys. Rev. B* **83** 235420

[12] Tseng M L, Hsiao H H, Chu C H, Chen M K, Sun G, Liu A Q and Tsai D P 2018 *Adv. Opt. Mater.* **6** 1800554

[13] Cui T, Bai B and Sun H B 2019 *Adv. Funct. Mater.* **29** 1806692

[14] Liu H, Lu J and Wang X R 2017 *Nanot.* **29** 024002

[15] Forouzmand A, Salary M M, Kafaie Shirmanesh G, Sokhoyan R, Atwater H A and Mosallaei H 2019 *Nanophotonics* **8** 415

[16] Choudhury S M, Wang D, Chaudhuri K, DeVault C, Kildishev A V, Boltasseva A and Shalaev V M 2018 *Nanophotonics* **7** 959

[17] Yin X H, Steinle T, Huang L L, Taubner T and Wuttig M 2017 *Light-Sci. Appl.* **6** e17016

[18] Bai W, Yang P, Wang S, Huang J, Chen D, Zhang Z, Yang J and Xu B 2019 *Appl. Sci.* **9** 4927

[19] Bai W, Yang P, Wang S, Huang J, Chen D, Zhang Z, Yang J and Xu B 2019 *Nanomaterials* **9** 993

[20] Chen L, Hao Y, Zhao L, Wu R, Liu Y, Wei Z, Xu N, Li Z and Liu H 2021 *Opt. Express* **29** 9332

[21] Chen W, Chen R, Zhou Y and Ma Y 2019 *IEEE Photon. Tech. Lett.* **31** 1187

[22] Wu J, Tang F, Ma J, Li Q, Shang S, Chen J, Wu Y, Wang Y, Ye X, Zheng W and Zhu R 2020 *Results Phys.* **18** 103226

[23] Butakov N A, Valmianski I, Lewi T, Urban C, Ren Z, Mikhailovsky A A, Wilson S D, Schuller I K and Schuller J A 2017 *ACS Photon.* **5** 371

[24] Rodriguez-Vega M, Simons M T, Radue E, Kittiwatanakul S, Lu J, Wolf S A, Lukaszew R A, Novikova I and Rossi E 2015 *Phys. Rev. B* **92** 115420

[25] Ordonez-Miranda J, Ezzahri Y, Joulain K, Drevillon J and Alvarado-Gil J J 2018 *Phys. Rev. B* **98** 075144

[26] Palik and Edward D 1985 *Handbook of optical constants of solids* (Maryland: Academic Press) pp. 554–769

[27] Shang S, Tang F, Ye X, Li Q, Li H, Wu J, Wu Y, Chen J, Zhang Z, Yang Y and Zheng W 2020 *Nanomaterials* **10** 103215

[28] Tang F, Ye X, Li Q, Wang Y, Yu H, Wu W, Li B and Zheng W 2020 *Results Phys.* **18** 103215